Full Paper
doi.org/10.1002/chem.202001365

Magnetic Anisotropy | *Hot Paper*

Highly Oxidized States of Phthalocyaninato Terbium(III) Multiple-Decker Complexes Showing Structural Deformations, Biradical Properties and Decreases in Magnetic Anisotropy

Yoji Horii[+],*[a] Marko Damjanović[+],*[b, g] M. R. Ajayakumar,[c] Keiichi Katoh,*[a] Yasutaka Kitagawa,[d] Liviu Chibotaru,[e] Liviu Ungur,[f] Marta Mas-Torrent,[c] Wolfgang Wernsdorfer,[g] Brian K. Breedlove,[a] Markus Enders,*[b] Jaume Veciana,*[c] and Masahiro Yamashita*[a, h, i]

Dedicated to Prof. Dr. Walter Siebert

Abstract: Presented here is a comprehensive study of highly oxidized multiple-decker complexes composed of Tb^{III} and Cd^{II} ions and two to five phthalocyaninato ligands, which are stabilized by electron-donating *n*-butoxy groups. From X-ray structural analyses, all the complexes become axially compressed upon ligand oxidation, resulting in bowl-shaped distortions of the ligands. In addition, unusual coexistence of square antiprism and square prism geometries around metal ions was observed in +4*e* charged species. From paramagnetic ^{1}H NMR studies on the resulting series of triple, quadruple and quintuple-decker complexes, ligand oxidation leads to a decrease in the magnetic anisotropy, as predicted from theoretical calculations. Unusual paramagnetic shifts were observed in the spectra of the +2*e* charged quadruple and quintuple-decker complexes, indicating that those two species are actually unexpected triplet biradicals. Magnetic measurements revealed that the series of complexes show single-molecule magnet properties, which are controlled by the multi-step redox induced structural changes.

Introduction

Extended π-systems[1] have versatile physical properties, such as redox, light absorption and emission, and electroconductivity, necessary for solar cells,[2] organic light-emitting diodes,[3] electro-batteries[4,5] and so on. There are two kinds of π-extensions: in-plane extension, and π–π stacking.[6] The bottom up synthesis of graphene nano-ribbons[7,8] and the construction of

[a] *Dr. Y. Horii,[+] Prof. Dr. K. Katoh, Prof. Dr. B. K. Breedlove, Prof. Dr. M. Yamashita*
Department of Chemistry, Graduate School of Science
Tohoku University
6-3 Aramaki-Aza-Aoba Aoba-ku, Sendai, Miyagi, 980-8578 (Japan)
E-mail: yoji.horii.c5@tohoku.ac.jp
keiichi.katoh.b3@tohoku.ac.jp

[b] *Dr. M. Damjanović,[+] Prof. Dr. M. Enders*
Institute of Inorganic Chemistry, Heidelberg University
Im Neuenheimer Feld 270, 69120 Heidelberg (Germany)
E-mail: markus.enders@uni-heidelberg.de

[c] *Dr. M. R. Ajayakumar, Prof. Dr. M. Mas-Torrent, Prof. Dr. J. Veciana*
Department of Molecular Nanoscience and Organic Materials
Institut de Ciencia de Materials de Barcelona (ICMAB-CSIC)/CIBER-BBN
08193 Bellaterra (Spain)
E-mail: vecianaj@icmab.es

[d] *Prof. Dr. Y. Kitagawa*
Department of Materials Engineering Science
Graduate School of Engineering Science, Osaka University
1-1 Machikaneyama-cho, Toyonaka, Osaka 560-8531 (Japan)

[e] *Prof. Dr. L. Chibotaru*
Theory of Nanomaterials Group, Katholieke Universiteit Leuven
3001 Leuven (Belgium)

[f] *Dr. L. Ungur*
Department of Chemistry, National University of Singapore
3 Science Drive 3, 117543 Singapore (Singapore)

[g] *Dr. M. Damjanović,[+] Prof. Dr. W. Wernsdorfer*
Institute of Nanotechnology (INT)
Karlsruhe Institute of Technology (KIT)
Hermann-von-Helmholtz-Platz 1
76344 Eggenstein-Leopoldshafen (Germany)
E-mail: marko.damjanovic@kit.edu

[h] *Prof. Dr. M. Yamashita*
School of Materials Science and Engineering, Nankai University
Tianjin 300350 (P. R. China)

[i] *Prof. Dr. M. Yamashita*
WPI-Advanced Institute for Materials Research, Tohoku University
2-1-1 Katahira, Sendai 980-8577 (Japan)
E-mail: masahiro.yamashita.c5@tohoku.ac.jp

[+] *These authors contributed equally to this work.*

Supporting information and the ORCID identification number(s) for the author(s) of this article can be found under: https://doi.org/10.1002/chem.202001365.

porphyrin tapes[9] are representative examples with in-plane extended π-systems, in which the precisely designed monomer units are connected regularly with sp^2 bonds, making it possible to control the morphology and the physical properties of the resulting products. Longitudinal infinite stacking of π-conjugated molecules is often seen in crystals of molecular conductors[10–13] and polymeric chains in which phthalocyanine (Pc) and/or porphyrin (Por) ligands are connected by siloxanes,[14] ligand–metal coordination bonds,[15] weak intermolecular interactions[16] and so on. In addition to infinite stacks, the development of Pc and Por chemistry has enabled the construction of stable oligomeric molecules with stacked π-systems.[17,18]

A series of phthalocyaninato-lanthanide-cadmium multiple-decker complexes[19–21] is a rare example of such oligomers (Figure 1). Lanthanoid-phthalocyaninato double- and triple-decker complexes were first prepared by Kirin et al. in 1965[22] and in 1967,[23,24] respectively, and were followed by the synthesis of their porphyrinato analogues reported by Buchler et al.[25] The first discrete phthalocyaninato quadruple-decker complex, in which two Lu^{III}-Pc double-decker complexes are glued by Cd^{II} ions, resulting in the tetrameric Pc stack connected by Lu-Cd-Lu metal array, was reported by Fukuda et al. in 2011.[26] Jiang et al. has further extended this strategy and reported quintuple- and sextuple-decker complexes in a short period of time.[20,21]

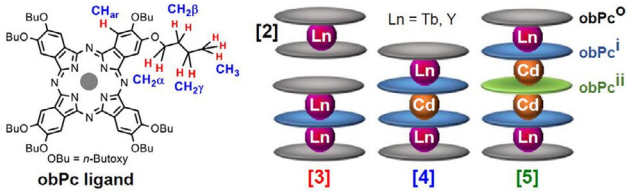

Figure 1. Schematic representation of structures and naming convention of the phthalocyaninato multiple-decker complexes in this work. obPc ligands can be distinguished as either inner ($obPc^i$ and, for the central ligand in **[5]**, $obPc^{ii}$) and outer ($obPc^o$). The chemical group annotations used for the solution NMR analysis are also summarized.

Among multiple-decker complexes, double-decker complexes are the most thoroughly studied, and several versatile functionalities related to future applications have been reported. For instance, redox induced structural changes of Por double-decker complexes have been utilized for rotating units of various molecular machines.[27–30] More recently, Yamashita et al. have observed structural changes in Por double-decker complexes induced by ligand oxidation using single-crystal X-ray (SXRD) measurements and have shown that ligand oxidation induces axial compression, which has been supported by theoretical calculations.[31] Moreover, the axial compression in Pc double-decker complexes induced by oxidation has been investigated by using solution NMR spectroscopy.[32] The conformational changes, especially ligand rotation, in double-decker complexes have been directly observed[33,34] and controlled using a scanning electron microscope (STM) and scanning electron spectroscopy (STS). In other words, bits of single-molecule memory using double-decker complexes has been achieved.[35] Moreover, double-decker complexes with Tb^{III} ions are outstanding SMMs[36] and have been used in spintronic devices, wherein the interactions between the spins of Tb^{III} ions, conductive electrons and phonons of nanocarbon materials are utilized.[37,38] Ishikawa et al. have reported a significant enhancement of the SMM properties of the Tb^{III}-phthalocyaninato double-decker complexes via the axial compression induced by the ligand oxidation.[39–41] In comparison with double-decker complexes, the redox, structural and magnetic properties of the other multiple-decker complexes have not been investigated as extensively presumably because they have short histories and low-profiles, are difficult to synthesize and purify and have low crystallinity. However, the more extended π-systems, as compared with double-decker complexes, are promising for bringing about valuable and unprecedented functionalities. For instance, Fukuda et al. have reported that the oxidized form of the quadruple-decker complex absorbs light in the longer wavelength regions, which is useful for light-harvesting materials in dye-sensitized solar cells.[42] In addition, non-linear optical properties of multiple-decker complexes have been investigated by Jiang et al.[21] From the point of view of molecular magnetism, various groups have utilized the multiple-decker complexes with two Tb^{III} and Dy^{III} centers for analyzing the effects of intramolecular magnetic interactions which affect the SMM properties.[26,43–46]

Herein we present an extensive study of oxidized π-extended multiple-decker oligomers, which were obtained through electrochemical and chemical oxidation reactions, utilizing single crystal X-ray diffraction (SCXRD), ESR, NMR, magnetic measurements and theoretical calculations. By using bulk electrolysis and UV/Vis/NIR measurements, we isolated and characterized the charged states of multiple-decker complexes. For concise naming, we use the number of 2,3,9,10,16,17,23,24-octabutoxy phthalocyaninato (obPc) ligands contained in the complex as ***[n]***, i.e., double- **[2]**, triple **[3]**, quadruple- **[4]** and quintuple-decker **[5]** complexes, and the charge of the complex (m) is expressed as $[n]^{m+}$, e.g., $+2e$ charged triple-decker complex is named $[3]^{2+}$. From the crystal structures of $[3]^{2+}$, $[4]^{2+}$, $[4]^{4+}$ and $[5]^{4+}$, it was shown that both molecular and packing structures were controlled by the size of the molecules and the numbers of counter ions. In addition, unusual coexistence of square prism (SP) and square antiprism (SAP) geometries were observed in $+4e$ charged species. Paramagnetic NMR analysis was used to characterize the structures and magnetic properties of the oxidized complexes in solution, and we showed that magnetic anisotropy decreased with an increase in the charges on the obPc ligands. Furthermore, although $[4]^{2+}$ and $[5]^{2+}$ have even positive charges, the existence of π-radicals was proven by NMR and ESR spectroscopies and supported by DFT calculations. In addition, we report the magnetic properties of the multiple-decker complexes which are shown to be influenced by the structural changes induced by oxidation of the ligand.

Results and Discussion

Isolation and characterization of oxidized multiple-decker complexes

The multiple-decker complexes were stepwise oxidized by using cyclic voltammetry and chemical methods using phenoxathiin hexachloroantimonate (Ox·$SbCl_6$). UV/Vis/NIR spectroelectrochemistry was used to follow the oxidations. In the spectra of the oxidized species presented in this article, isosbestic points were observed (Figure 2d), indicating that the oxidized complexes are stable. The redox potentials became narrower (Figure 2b), and the number of stable oxidized species increased when the number of obPc ligands was increased because the π-system extension decreased the electronic repulsion between the positively charged holes. Since Tb^{III} and Cd^{II} ions do not participate in the redox reactions, the oxidation reactions occurred in the extended ligand π-system. The delocalization of holes is expected due to the highly delocalized molecular orbitals (Figure 2c). The agreement between the calculated oscillator strengths and absorption spectra support the validity of our calculations. The HOMO of the neutral species (Figure 2c) has nodes between the obPc ligands, indicating that ligand oxidation (i.e., removal of electrons from the HOMO) results in a decrease in the interligand distances. DFT optimized structures (Figures S246, S254, and S265) and crystal structures of oxidized species followed this trend as discussed later.

X-ray structural analysis

We obtained new crystal structures of $[\mathbf{3}]^{2+}$, $[\mathbf{4}]^{2+}$, $[\mathbf{4}]^{4+}$ and $[\mathbf{5}]^{4+}$, the crystals of which were grown by using chemical oxidations and a solvent diffusion method (see Supporting Information). The X-ray structures, including the previously reported structures of the neutral species ($[\mathbf{3}]^{0}$, $[\mathbf{4}]^{0}$ and $[\mathbf{5}]^{0}$)[43,44,47] are shown in Figures 3a–c.[48] The molecular length (*d*), stacking angle between the obPc ligands (θ_{obPc}) sandwiching the Tb^{III} ions, and the Tb^{III} to neighboring metal ion distance (R_{Tb-M}: M = Tb, Cd) from X-ray and DFT optimized structures are summarized in Figure 3d. In $[\mathbf{3}]^{0}$ and $[\mathbf{3}]^{2+}$, the two Tb^{III} ions are crystallographically equivalent and are connected by an inversion center (Figure 3a). In $[\mathbf{3}]^{0}$, *d*, R_{Tb-Tb} and θ_{obPc} were determined to be 6.095 Å, 3.517 Å and 31.77°, respectively. Oxidation to $[\mathbf{3}]^{2+}$, which corresponds to the removal of two electrons from the antibonding HOMO of $[\mathbf{3}]^{0}$ (Figure 2c), causes *d* and R_{Tb-Tb} (5.959 Å and 3.435 Å, respectively) to shorten, resulting in a square antiprism (SAP) geometry with a wide θ_{obPc} (42.21°) in order to avoid steric repulsion between the phenyl rings of the obPc ligands. Due to the large interligand steric effects induced by longitudinal compression, the outer obPcs ($obPc^{o}$) of $[\mathbf{3}]^{2+}$ had bowl-shaped distortions. The distortion and changes in the geometrical parameters (θ_{obPc}, *d* and R_{Tb-Tb}) are similar to those predicted from geometry optimization, as is summarized in Figure 3d.

In the case of series **[4]**, the space groups of $[\mathbf{4}]^{2+}$ and $[\mathbf{4}]^{4+}$ were determined to be *P4/ncc* and *P4/n*, respectively, and there are four-fold axes along the Tb-Cd-Tb axes (*c*-axes). Since the positional disorder in two obPcs of $[\mathbf{4}]^{4+}$ gave identical geometries in each disordered state, we only show one representative geometry on the right side of Figure 3b. Similar to the other multiple-decker series, in **[4]**, the $obPc^{o}$ ligands have bowl-shaped distortions induced by oxidation. In series **[4]**, although the two Tb^{III} ions are crystallographically inequivalent, the θ_{obPc} values of Tb1 and Tb2 (left side of Figure 3b) of $[\mathbf{4}]^{0}$ are similar to each other (22.32° and 23.65°). In $[\mathbf{4}]^{2+}$, θ_{obPc} of Tb1 and Tb2 are 42.28°and 38.72°, respectively. The differences in θ_{obPc} are greater in $[\mathbf{4}]^{4+}$, in which there are two θ_{obPc} (44.94° for Tb1 and 16.43° for Tb2). In other words, SAP and square-prism (SP) geometries are present in one $[\mathbf{4}]^{4+}$ unit. Since there are a small number of peaks in the ^1H NMR spectra of $[\mathbf{4}]^{4+}$ dissolved in CD_2Cl_2 due to its symmetric structure, the asymmetric crystal structure of $[\mathbf{4}]^{4+}$ seems to be induced by steric effects from the solvent molecules and $SbCl_6^-$ incorpo-

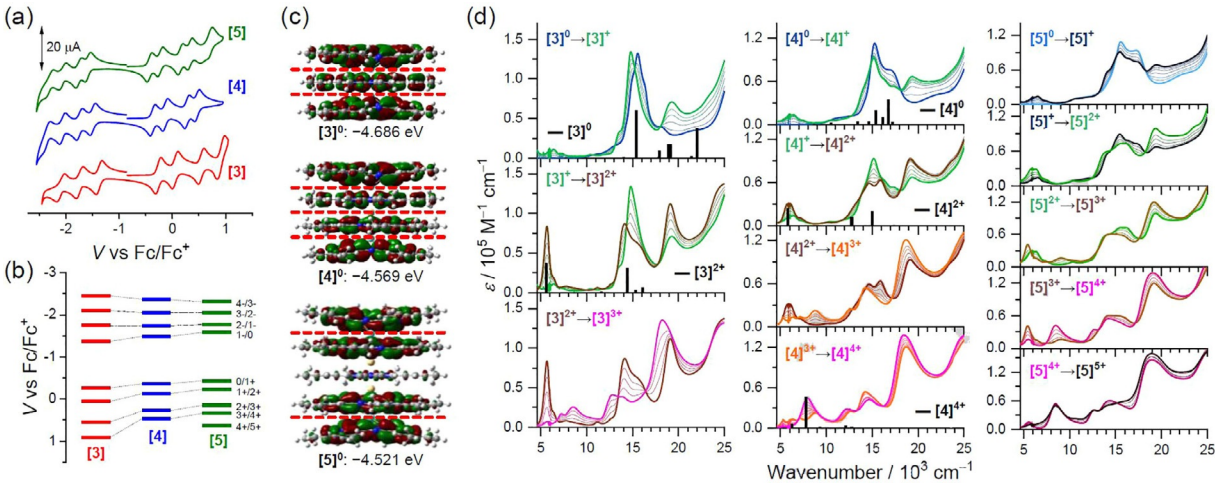

Figure 2. (a) Cyclic voltammograms,[44] (b) redox potentials, (c) HOMO (isovalue = 0.01) of neutral species and (d) electrochemical UV/Vis/NIR spectra and oscillator strength (black bars) for multiple-decker complexes.

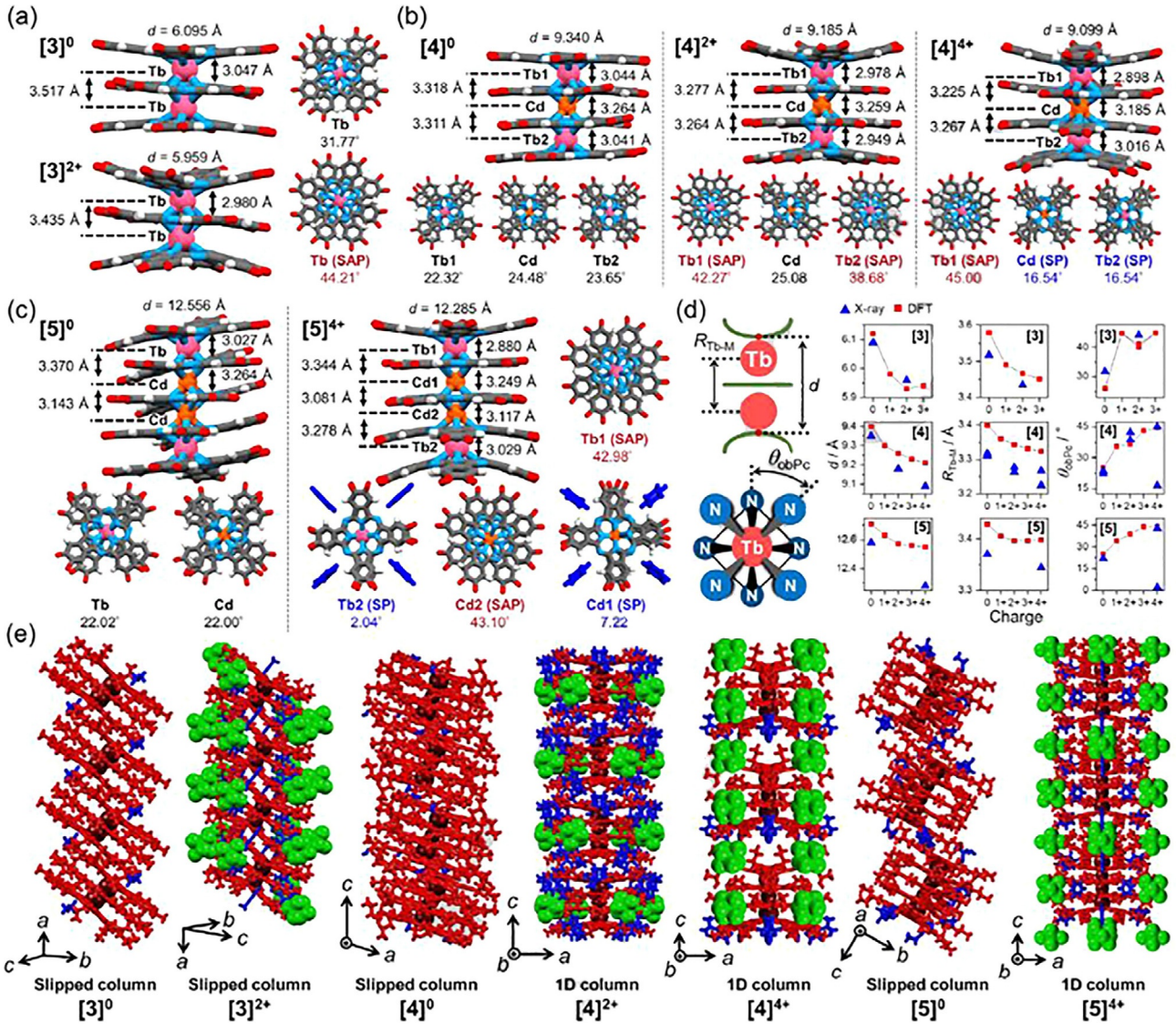

Figure 3. Crystal structures of (a) **[3]**, (b) **[4]** and (c) **[5]**. The *n*-butoxy chains were omitted for clarity. (d) Charge dependence of the molecular length *d*, Tb-metal ion (Tb or Cd) distances $R_{Tb\text{-}M}$ and stacking angle around metal ions θ_{obPc}. (e) Packing structures of multiple-decker complexes. Red, green and blue parts represent multiple-decker units, counter anions ($SbCl_6$) and solvent molecules, respectively.

rated into the crystal. The geometry optimization for $[\mathbf{4}]^{4+}$, by which the structure in the gas phase can be estimated, afforded the symmetric structure, further supporting the importance of intermolecular forces in the crystals to stabilize the asymmetric conformation observed by using SCXRD. We determined a preliminary crystal structure of $[\mathbf{4}]^{4+}$ crystalized from toluene, showing that the geometry of $[\mathbf{4}]^{4+}$ is independent of the conditions (SAP and SP geometries coexist as shown in Figure S310). Moreover, the SP conformations are stabilized by toluene molecules incorporated into the grooves of the obPc ligands.

In case of the structure of $[\mathbf{5}]^{4+}$, the obPc° ligands of $[\mathbf{5}]^{4+}$ show bowl-shaped distortions due to longitudinal compression effects induced by the oxidation in contrast to the wave-like distortions in $[\mathbf{5}]^{0}$. Although the Tb^{III} ions in $[\mathbf{5}]^{0}$ are crystallographically equivalent with each other, those in $[\mathbf{5}]^{4+}$ had different geometries, one of which was SAP and the other was SP. Moreover, the solvent molecules (benzene) located in the grooves formed by the ligands stabilize the SP geometry. Stacking of alternating $[\mathbf{5}]^{4+}$ and a disordered $SbCl_6^-$ generates 1D column packing along the *c*-axis (Figure 3e). At the same time, we determined the structure of $[\mathbf{5}]^{4+}$ containing toluene molecules obtained by slow diffusion using CH_2Cl_2 and toluene (Figures S302 and S303). Units of **[5]** with SAP and SP geometries are aligned into 1D column packing along the *c*-axis. Furthermore, the SP geometry is stabilized by toluene molecules incorporated to the groove of SP geometries (right side of Figure 3c). In other words, aromatic solvent molecules cause the coexistence of SAP and SP geometries in one multiple-decker unit. In all cases, the oxidation reactions resulted in compressions along the C_4 axes, followed by decreases in the steric hindrance due to bowl-shaped distortions of the obPc° ligands. The θ_{obPc} values increase when the complexes are oxidized from neutral ($\theta_{obPc} = 22°–32°$) to 2+ ($\theta_{obPc} = 38°–44°$) because

the wider θ_{obPc} decreases the steric hindrance between the cofacial ligands. In the cases of **[4]**$^{4+}$ and **[5]**$^{4+}$, there are two different Tb^{III} ions per molecular unit with $\theta_{obPc} \approx 45^\circ$ (SAP) and 0° (SP). Although the SP arrangement is unfavorable from the viewpoint of steric hindrance, aromatic solvent (benzene) molecules in the crystal packing of **[5]**$^{4+}$ stabilizes it. The structure of **[4]**$^{4+}$ with a narrow θ_{obPc} crystallized from toluene was also stabilized (Figure S305), indicating that both SAP and SP geometries generally occur in the crystal packing of highly oxidized species. Not only the molecular structures but also the crystal packings are controlled by oxidation. As shown in Figure 3e, the neutral species were packed in slipped column arrangements because of intermolecular π–π stacking. Moreover, **[3]**$^{2+}$ was packed in a slipped column arrangement because of its shorter *d*, which does not prevent the formation of π–π stacking. However, the oxidized forms of **[4]** and **[5]** were packed in 1D columns along the *c*-axis because of their larger dimensions along the *z*-axis and the bowl-shaped distortion of the obPc°, both of which prevent the formation of intermolecular π–π stacks.

Solution NMR measurements

Solution NMR is a useful tool to determine the molecular structures and magnetic properties of lanthanoid complexes.[49–50] The chemical shift of an NMR active nucleus in a paramagnetic complex can be expressed as the sum of the orbital term (δ_{orb}) and hyperfine term (δ_{HF}). δ_{HF} is mainly composed of the Fermi contact (δ_{FC}) and pseudocontact (δ_{PC}) shifts, as shown in Eq. (1):[51–52]

$$\delta_{obs} = \delta_{orb} + \delta_{HF} = \delta_{orb} + \delta_{FC} + \delta_{PC} \quad (1)$$

δ_{FC} involves the interactions between the electron spin on the nucleus and the nuclear spin, whereas δ_{PC} originates from the through-space magnetic dipole–dipole interactions between the electron magnetic moment and the nuclear magnetic moment.[53] Both metal ions and ligand-centered π-radicals can contribute to δ_{HF}. In lanthanoid complexes, δ_{PC} due to the metal ion is the dominant term when the anisotropy is high. The Tb^{III} ions in the present complexes are affected by the ligand field of the obPc ligands, and therefore, the Tb^{III} ions have strong axial magnetic anisotropies with the magnetic easy axes lying along the C_4 axes of the multiple-decker complexes.[54] In this case, theδ_{PC} due to the metal ion (δ_{MPC})[49] is the dominant term and can be expressed as [Eq. (2)]:

$$\delta_{MPC} = \frac{\chi_{ax}}{12\pi r^3}(3\cos^2\theta - 1) \quad (2)$$

in which χ_{ax} is the axial component of the magnetic susceptibility of the lanthanoid center, *r* is the norm of the vector (*r*) connecting the lanthanoid center and the nucleus, θ is the angle between the magnetic easy axis and the *r* (Figure S29). Previously, we have concluded that the decrease in the molecular length (*d*) and the increase in χ_{ax} value contribute to the larger δ_{MPC} induced by ligand oxidation in Tb^{III}-phthalocyanine to double-decker complexes (**[2]**).[32] Moreover, the increases in the magnetic anisotropy via ligand oxidation are supported by the ac magnetic properties of the cationic double-decker complexes in the solid state reported by Ishikawa et al.[39–41] However, in contrast to δ_{MPC} for **[2]**, that for the series of complexes **[3]**–**[5]** in the present research did not increase simply with an increase in the oxidation state of the ligand.

The ^{1}H NMR signals were fully assigned using a combination of ^{1}H NMR and ^{1}H-^{1}H COSY spectra and an estimation of δ_{MPC} using DFT optimized structures. As shown in Figure 4, the ^{1}H signals for CH_{ar} changed complicatedly upon oxidation. In contrast, the paramagnetic shift of most of the signals for $CH_2\alpha$, $CH_2\beta$, $CH_2\gamma$ and CH_3 decreased with an increase in the oxidation number, which is indicative of a decrease in $c_{ax}.\delta_{obs}$ for the CH_{ar} protons heavily depended on the ligand contribution to δ_{FC} (δ_{LFC}) because these protons were close to the π-radicals. Thus, the chemical shift of CH_{ar} (δ_{obs}^{ar}) is simplified as the sum of δ_{MPC}, δ_{LFC} and less charge dependent δ_{orb}, as shown below. [Eq. (3)]

$$\delta_{obs}^{ar} \approx \delta_{orb} + \delta_{MPC} + \delta_{LFC} \quad (3)$$

δ_{LFC} for CH_{ar} was estimated using the spin densities at measured nuclei obtained from DFT calculations.[32] The spin densities on the CH_{ar} of obPc° tend to be high compared to those of obPc^i, and thus, the magnitude relation of δ_{obs}^{ar} for CH_{ar}^{o} and CH_{ar}^{i} changes upon oxidation of the ligand, as seen in the ^{1}H NMR spectra of **[4]** and **[5]** beyond −55 ppm. In contrast to CH_{ar}, the protons of the butoxy chains are less affected by the π-radicals and charges on the ligands because these protons are far from the π-plane, making it possible to treat δ_{FC} as being zero.[32] Using the equation above and the DFT-optimized structures of the oxidized complexes to which *n*-butoxy chains were added (Figure S247, S255 and S266), the χ_{ax} values were determined by least-squares fitting as to minimize the difference in the observed and expected chemical shifts (δ_{obs} and δ_{calcd}, respectively). The χ_{ax} values of the multiple-decker complexes are shown in Figure 5b. Except the increase in the χ_{ax} value upon oxidation from **[3]**$^{2+}$ to **[3]**$^{3+}$, χ_{ax} values of the multiple-decker complexes decreased with an increasing the number of charges on the ligands, indicating that the magnetic anisotropy decreased due to changes induced by chemical oxidation. Another point to be mentioned is the paramagnetic shift for the CH_{ar}^{o} protons in **[4]**$^{2+}$ and **[5]**$^{2+}$ (centre of Figure 5a). Since they have even charges, the ligand π-radical and resulting δ_{LFC} are expected to be absent, and only δ_{MPC} is the source of the paramagnetic shift. However, the observed chemical shifts for adding δ_{LFC} obtained from DFT calculations for triplet states of **[4]**$^{2+}$ and **[5]**$^{2+}$ to d_{obs}^{ar}, affording shifts of −102.9 ppm and −105.9 ppm for **[4]**$^{2+}$ and **[5]**$^{2+}$, respectively, which are close to the experimental values. The remaining differences of about −10 ppm are due to the contribution of singlet states and the pseudocontact shift contributions of the organic radicals, as has been shown by more elaborate analysis.[54,55]

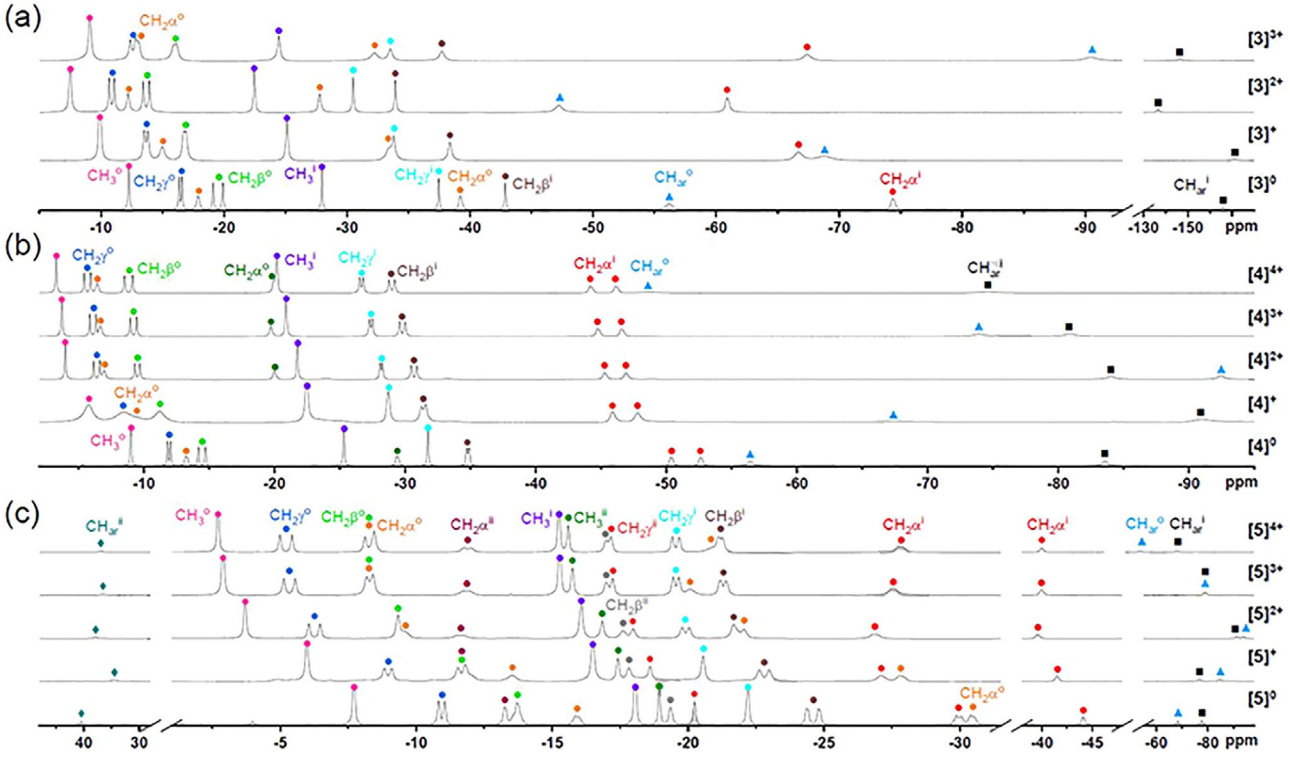

Figure 4. ^{1}H NMR spectra for oxidized and neutral species of (a) **[3]**, (b) **[4]** and (c) **[5]** with the assignment of the signals at 295.0 K.

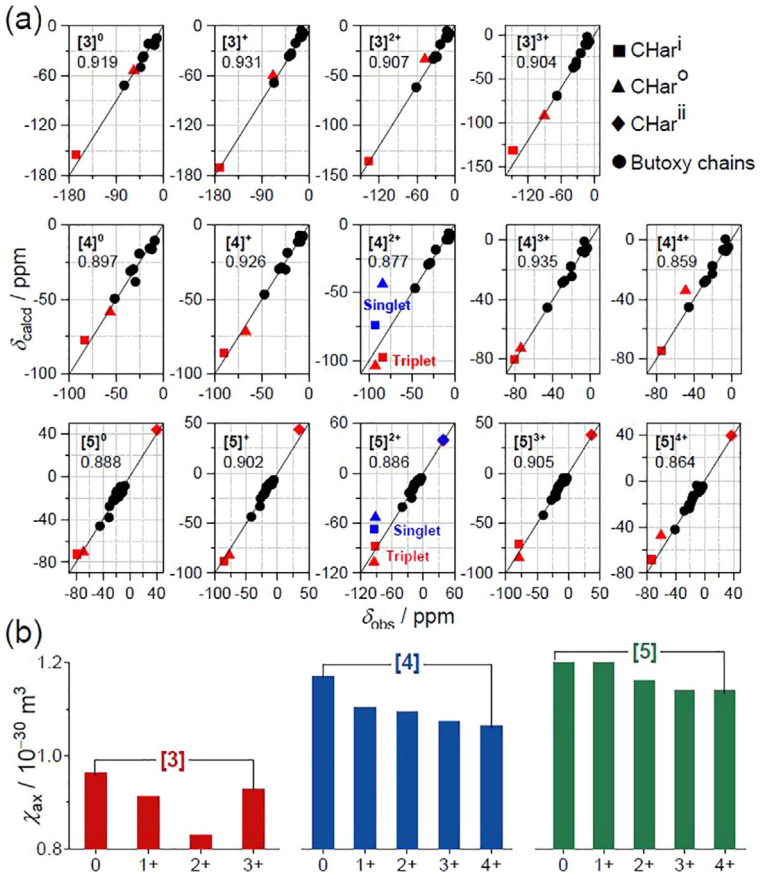

Figure 5. (a) Relationship between the δ_{obs} and δ_{calcd}, expressed with the agreement factor written under the abbreviation of the complex (with consideration of singlet and triplet states, where appropriate). Numbers are agreement factors (*AF*s) using $AF = 1-[\Sigma(\delta_{calcd}-\delta_{obs})^2/\delta_{obs}{}^2]^{1/2}$. (b) χ_{ax} values for the series **[3]**, **[4]** and **[5]** derived from ^{1}H NMR analysis at 295 K.

Biradical properties of $[4]^{2+}$ and $[5]^{2+}$

From the NMR analysis, in $[4]^{2+}$ and $[5]^{2+}$, the π-radicals are on the ligands, especially on obPc°. However, the relatively sharp ^{1}H NMR signals in the spectra of $[4]^{2+}$ and $[5]^{2+}$ compared to those of other radical complexes indicates that there are contributions from singlet (π-radical silent) states as well. To support the presence of π-radicals, we performed electron spin resonance (ESR) spectroscopy on Y(III) analogues of the oxidized complexes, which were prepared via bulk electrolysis in CH_2Cl_2 and characterized by comparing their absorption spectra with those of Tb^{III} complexes (Figure S319). Although Y(III) analogues of $[4]^{2+}$ and $[5]^{2+}$ have even charges, these complexes are ESR active at room temperature, and their *g*-values are close to 2, which is common for organic radicals. After cooling to 80 K, in the ESR spectra of $[4]^{2+}$ and $[5]^{2+}$, complicated signals, which were characteristic of a triplet biradical with an axial zero-field splitting parameter *D*, were observed (Figure 6b, S316, S317). The simulated $|D|$ value for $[4]^{2+}$ (0.0032 cm^{-1}) is slightly larger than that for $[5]^{2+}$ (0.0029 cm^{-1}), indicating that $[4]^{2+}$ has stronger dipole-dipole interactions between unpaired electrons than $[5]^{2+}$ does due to the smaller π-extended system in the former compound. Focusing on the shape and energy of the molecular orbitals in the even-charged complexes, HOMO–LUMO gaps ($\Delta E_{LUMO-HOMO}$ as shown Figure 6c) for $[4]^{2+}$ and $[5]^{2+}$ (0.20 and 0.14 eV, respectively) are considerably smaller than those for others (0.47 to 1.21 eV) because the HOMO and LUMO of $[4]^{2+}$ and $[5]^{2+}$ are non-bonding orbitals whose shapes are similar with each other (S259, S270). The small $\Delta E_{LUMO-HOMO}$ for $[4]^{2+}$ and $[5]^{2+}$ allows the electrons to occupy the LUMO with low energy, resulting in the formation of biradical states. To better understand the biradical states, we performed natural orbital (NO) analysis on antiferromagnetic (AFM) states using (U)B3LYP/6-31G*[56–58] with Stuttgart RSC 1997 ECP[59] for Y and Cd ions (see Supporting Information). The occupancies of the lowest unoccupied natural orbitals (LUNO) for the singlet states of $[4]^{2+}$ and $[5]^{2+}$ were 0.922 and 0.961, respectively. In addition, diradical character *y* values for $[4]^{2+}$ and $[5]^{2+}$ were 0.845 and 0.922, respectively, indicating that there are contributions from triplet ferromagnetic (FM) states. The calculated exchange interactions (J_{ex}) between the two $S=1/2$ spins of $[4]^{2+}$ and $[5]^{2+}$ were -34 cm^{-1} and -3 cm^{-1}, respectively, the magnitudes of which are small enough for the triplet (ferromagnetic) states to be thermally accessible at liquid nitrogen temperatures. These results are consistent with the triplet biradical states observed using ESR measurements at 80 K.

So far, biradical compounds with Pc and Por have been synthesized by connecting two neutral double-decker monoradical complexes.[54,60–63] Among them, a triplet biradical state has been reported for a K^+ ion-induced supramolecular tetramer composed of crown-substituted double-decker complexes, $[K_4\{Lu(CR_4Pc)Pc\}_2]^{4+}$, reported by Ishikawa et al., where the four phthalocyaninato ligands align along the C_4 axis to make a purely longitudinally extended π-system.[61] From empirical calculations, $[K_4\{Lu(CR_4Pc)Pc\}_2]^{4+}$ has a small negative J_{ex} value (-0.35 cm^{-1}). In contrast, connecting the two double-decker complexes via an in-plane π-extended ligand, such as fused-phthalocyanine FPc[54] or fused-porphyrin FPor,[62,63] results in the formation of a singlet biradical species showing strong antiferromagnetic interactions between $S=1/2$ spins (-207.4 cm^{-1} and -487 cm^{-1}, respectively). Weak J_{ex} values for $[4]^{2+}$ and $[5]^{2+}$ in the present study are similar to that for $[K_4\{Lu(CR_4Pc)Pc\}_2]^{4+}$. J_{ex} tends to be weak when the biradicals occur in π–π stacks (Figure 6d). These results clearly reflect the differences in orthogonality of interligand orbital overlap, which is retained in the longitudinally extended π-system with wide interligand stacking angles θ.

Correlations between the magnetic anisotropy and the redox-induced structural changes

From NMR analyses of the oxidized species, the magnetic anisotropy (χ_{ax}) on the Tb^{III} ion decreased upon oxidation. To determine the correlation between the structural deformation caused by ligand oxidation and the magnetic anisotropy, we performed point-charge (PC) calculations. Although PC calculations are less accurate than ab initio methods are, its low computation cost makes it possible to estimate the ligand field (LF) splitting of the present lanthanoid complexes having large numbers of atoms and metal centers. Since Tb–N and Cd–N bonds have covalent character, the negative charges on the coordinating N atoms should extend in Tb(Cd)–N direction. Using PC calculations with the displacement parameters sug-

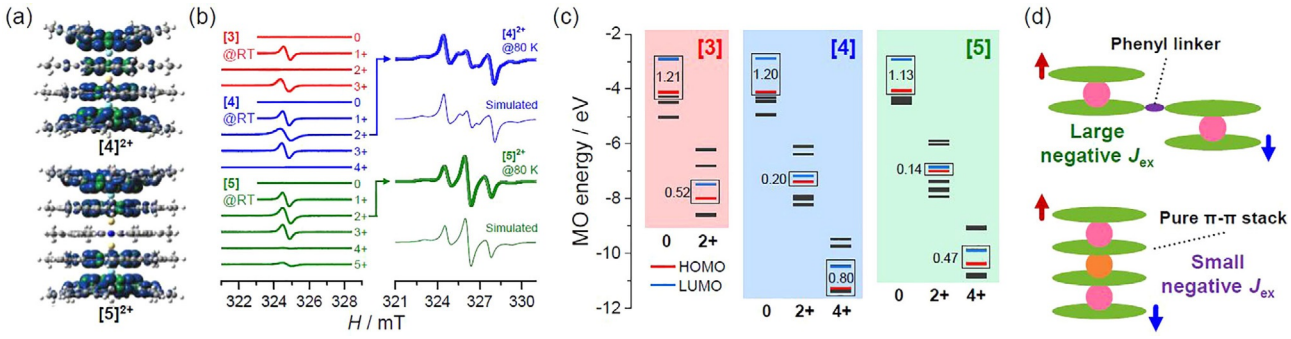

Figure 6. (a) Spin densities (isovalue = 0.004) of triplet biradical species. (b) EPR spectra of Y(III) analogues at RT (experimental) and at 80 K (experimental and simulated). (c) Molecular orbital energies and HOMO–LUMO gaps of singlet species. (d) Comparison of J_{ex} values between the dimer of double-decker complexes connected by a phenyl linker and the double-decker complexes connected by π–π stacking.

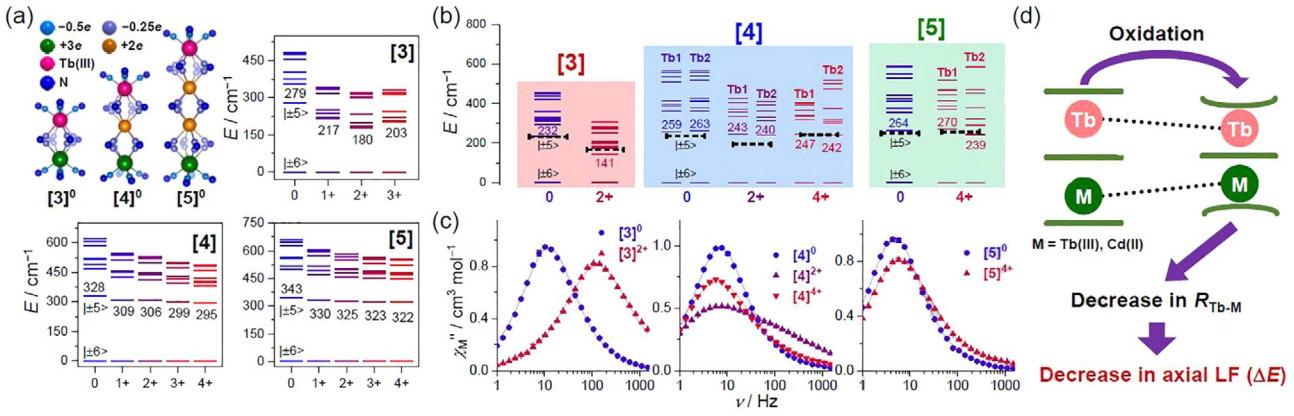

Figure 7. (a) Crystal field splitting and structural model of neutral species based on point-charge calculations done on the DFT-optimized structures. (b) Ligand field splitting of multiple-decker complexes by CASSCF[64] calculations using the crystal coordination fragment around Tb^{III} ions. Two kinds of energy levels are shown in cases when crystallographically inequivalent Tb^{III} ions are present. Dotted lines represent experimental ΔE values estimated by ac magnetic susceptibility measurements in the presence of a dc bias magnetic field. (c) Selected ac magnetic susceptibilities at 10 K with a 2 kOe bias dc field. (d) Mechanism for the decrease in ΔE upon oxidation.

gested by Baldoví et al.,[65] the effects of the covalent bonds between the phthalocyaninato ligands and metal ions can be considered. As is shown in Figures 7a and S308, we constructed the structural models for the PC calculations on the bases of the DFT-optimized structures of the oxidized complexes and the reported displacement parameters,[65] which shift the positions of the negative charge of the coordinated N atoms closer to the metal ions. Since the obPc° ligand is tetradentate with a$-2e$ charge, a$-0.5e$ charge was assigned per coordinated N atom. In a similar manner, a$-0.25e$ charge was assigned to each metal–N bond since each N atom of obPc^{i} coordinates to two metal ions. In addition, Cd^{II} ions and the Tb^{III} ions on the opposite side of were treated as $+2e$ and $+3e$ point charges, respectively. From PC calculations using these models, the ground states of the multiple-decker complexes were composed of $|J_z>=|\pm6>$ similar to the well-studied phthalocyaninato Tb^{III} double-decker complexes.[36] Moreover, the energy separation between the LF sublevels (magnitude of the LF splitting) successively decreased due to the structural deformation induced by oxidation (Figure 7a), which consistent with the decrease in the χ_{ax} values observed from NMR analysis. In addition, the LF splitting is enhanced by the structural changes upon oxidation from $\mathbf{[3]}^{2+}$ to $\mathbf{[3]}^{3}$ (Figure 5b). These simple calculations indicate that the χ_{ax} values obtained from the NMR measurements depend on the LF splitting of the Tb^{III} ions and are modulated by redox-induced structural changes. In particular, the negative charges of three obPc ligands must be included to reproduce the increase in the LF splitting upon oxidation from $\mathbf{[3]}^{2+}$ to $\mathbf{[3]}^{3+}$. The decrease in the LF splitting upon oxidation is more pronounced for **[3]** than it is for **[4]** and **[5]**. To further understand the behavior of the χ_{ax} values and LF splitting, we conducted magnetic measurements on the oxidized species characterized by X-ray analysis. Since the Tb^{III} ions have strong magnetic anisotropy (large χ_{ax} value), the multiple-decker complexes underwent slow magnetic relaxations characteristics of SMMs, as shown by the imaginary part of the ac magnetic susceptibility (χ_M'') vs. ac frequency (ν) plots (Figure 7c). Among the studied complexes, χ_M'' of **[3]** clearly shifted toward the higher ν region as the oxidation state increased. In contrast, the peak top of χ_M'' for the other species are less dependent on their oxidation states. In other words, the magnetic relaxation time (τ) of **[3]** strongly correlates with the oxidation state. The activation energies for spin reversal (ΔE), which correspond to the energy difference between the highly anisotropic ground doublet $|\pm6>$ and the first excited LF levels $|\pm5>$, were determined by fitting τ vs. T^{-1} plots using Arrhenius equations (magnetic section in Supporting Information). In addition, ab initio calculations using the crystal structures around the Tb^{III} ions were performed to determine the LF splitting (Figure 7b and the details of ab initio calculations in Supporting Information). We found that there was agreement between the experimental ΔE values (dotted lines in Figure 7b) and theoretical LF splitting. In particular, the ΔE values for series **[3]** decreased as the complexes were oxidized from $\mathbf{[3]}^{0}$ to $\mathbf{[3]}^{2+}$, the trend of which is consistent with the decrease in χ_{ax} values obtained from NMR analyses and PC calculations. We think that the approach of the Tb^{III} ions (decrease in R_{Tb-M} shown in Figure 3d) via axial compressions induced by ligand oxidation decrease the effects of the negative charges on the inner ligands (obPc^{i}), and therefore, the axial components of the LF parameters around the Tb^{III} ions decrease (Figure 7d). In comparison to **[3]**, the other complexes with Cd^{II} ions do not show large changes in the ac magnetic properties and LF splitting upon ligand oxidation owing to the approach of the less positively charged Cd^{II} ion to the Tb^{III} ions.

Conclusions

We showed the versatile electrochemical, magnetic and structural properties of highly oxidized multiple-decker complexes. The ligand oxidation state and the magnetic properties of the lanthanoid center couple with each other due to structural deformations. Stepwise oxidation, possible in the present series of complexes, could lead to multistep molecular switches,

which would be useful as molecular magnets and in molecular machines. Not only could the structural deformations and changes in magnetic properties be controlled, but also a strategy to synthesize new dicationic biradical species was discovered. Longitudinal extension of the π-plane with electron donating groups and a two electron oxidation results in the exceptionally low HOMO–LUMO energy gaps and spin densities distributed mostly on the outer ligands. By extending the stacked π-structure, the distance between the monoradical spin units increases, although they are connected by the π-plane. We believe that the controlled loss of two electrons from π-stacked molecular wires will lead to huge triplet biradical species, making these materials interesting both for their conductive and light-harvesting properties.

Supporting Information contains details in magnetic properties, quantum chemical calculations, NMR and ESR analysis.

Acknowledgements

This work was financially supported by the Japan Society for the Promotion of Science (JSPS) KAKENHI Grant Numbers JP14J02656 (Y.H.), JP20225003 (M.Y.), JP15K05467 (K.K.), JP24750119 (K.K.), 18K14242 (Y.H.), 19K05401(Y.K), Tohoku University Molecule & Material Synthesis Platform in Nanotechnology Platform Project, CREST, JST JPMJCR12L3 (M.Y.), PhD scholarship from the Beilstein-Institut zur Förderung der Chemischen Wissenschaften (M.D.), the German-Japanese University Consortium (HeKKSaGOn), the state of Baden-Württemberg through bwHPC and the German Research Foundation (DFG) through grant no INST 40/467-1 FUGG (JUSTUS cluster), European Union (ERC StG 2012–306826 e-GAMES), Networking Research Center on Bioengineering, Biomaterials, and Nanomedicine (CIBER-BBN), the Spanish Ministry of Economy and Competitiveness (projects FANCY CTQ2016-80030-R, MOTHER MAT2016-80826-R and the "Severo Ochoa" Programme for Centers of Excellence in R&D, SEV-2015-0496), Generalitat de Catalunya (2017SGR918), 111 Project (B18030) from China (M.Y.), the scientific grants R-143-000-A80-114, R-143-000-A65-133 from the National University of Singapore. We thank Dr. Norihisa Hoshino for EPR measurements, Dr. Tetsuko Nakaniwa and Prof. Dr. Genji Kurisu and Dr. Takefumi Yoshida for SCXRD measurements. This paper is Contribution No. 62 from the Research Center for Thermal and Entropic Science.

Conflict of interest

The authors declare no conflict of interest.

Keywords: biradical · crystal engineering · magnetic anisotropy · NMR · redox

[1] V. V. Roznyatovskiy, C.-H. Lee, J. L. Sessler, *Chem. Soc. Rev.* **2013**, *42*, 1921 – 1933.
[2] Y.-J. Cheng, S.-H. Yang, C.-S. Hsu, *Chem. Rev.* **2009**, *109*, 5868 – 5923.
[3] A. C. Grimsdale, K. Leok Chan, R. E. Martin, P. G. Jokisz, A. B. Holmes, *Chem. Rev.* **2009**, *109*, 897 – 1091.
[4] Y. Morita, S. Nishida, T. Murata, M. Moriguchi, A. Ueda, M. Satoh, K. Arifuku, K. Sato, T. Takui, *Nat. Mater.* **2011**, *10*, 947.
[5] C. Wang, Y. Xu, Y. Fang, M. Zhou, L. Liang, S. Singh, H. Zhao, A. Schober, Y. Lei, *J. Am. Chem. Soc.* **2015**, *137*, 3124 – 3130.
[6] C. A. Hunter, J. K. M. Sanders, *J. Am. Chem. Soc.* **1990**, *112*, 5525 – 5534.
[7] A. Narita, X.-Y. Wang, X. Feng, K. Müllen, *Chem. Soc. Rev.* **2015**, *44*, 6616 – 6643.
[8] Y. Yano, N. Mitoma, K. Matsushima, F. Wang, K. Matsui, A. Takakura, Y. Miyauchi, H. Ito, K. Itami, *Nature* **2019**, *571*, 387 – 392.
[9] A. Tsuda, A. Osuka, *Science* **2001**, *293*, 79 – 82.
[10] J. Ferraris, D. O. Cowan, V. Walatka, J. H. Perlstein, *J. Am. Chem. Soc.* **1973**, *95*, 948 – 949.
[11] J. L. Petersen, C. S. Schramm, D. R. Stojakovic, B. M. Hoffman, T. J. Marks, *J. Am. Chem. Soc.* **1977**, *99*, 286 – 288.
[12] P. Cassoux, L. Valade, H. Kobayashi, A. Kobayashi, R. A. Clark, A. E. Underhill, *Coord. Chem. Rev.* **1991**, *110*, 115 – 160.
[13] A. Kobayashi, E. Fujiwara, H. Kobayashi, *Chem. Rev.* **2004**, *104*, 5243 – 5264.
[14] J. B. Davison, K. J. Wynne, *Macromolecules* **1978**, *11*, 186 – 191.
[15] M. Hanack, A. Hirsch, H. Lehmann, *Angew. Chem. Int. Ed. Engl.* **1990**, *29*, 1467 – 1468; *Angew. Chem.* **1990**, *102*, 1499 – 1501.
[16] K. Venkata Rao, D. Miyajima, A. Nihonyanagi, T. Aida, *Nat. Chem.* **2017**, *9*, 1133 – 1139.
[17] T. R. Janson, A. R. Kane, J. F. Sullivan, K. Knox, M. E. Kenney, *J. Am. Chem. Soc.* **1969**, *91*, 5210 – 5214.
[18] A. B. Anderson, T. L. Gordon, M. E. Kenney, *J. Am. Chem. Soc.* **1985**, *107*, 192 – 195.
[19] T. Fukuda, T. Biyajima, N. Kobayashi, *J. Am. Chem. Soc.* **2010**, *132*, 6278 – 6279.
[20] H. Wang, N. Kobayashi, J. Jiang, *Chem. Eur. J.* **2012**, *18*, 1047 – 1049.
[21] H. Wang, D. Qi, Z. Xie, W. Cao, K. Wang, H. Shang, J. Jiang, *Chem. Commun.* **2013**, *49*, 889 – 891.
[22] I. S. Kirin, P. N. Moskalev, Y. A. Makashev, *Russ. J. Inorg. Chem.* **1965**, *10*, 1065 – 1066.
[23] I. S. Kirin, P. N. Moskalev, N. V. Ivannikova, *Russ. J. Inorg. Chem.* **1967**, *12*, 497 – 498.
[24] I. S. Kirin, P. N. Moskalev, Y. A. Makashev, *Russ. J. Inorg. Chem.* **1967**, *12*, 369 – 372.
[25] J. W. Buchler, A. De Cian, J. Fischer, M. Kihn-Botulinski, H. Paulus, R. Weiss, *J. Am. Chem. Soc.* **1986**, *108*, 3652 – 3659.
[26] T. Fukuda, W. Kuroda, N. Ishikawa, *Chem. Commun.* **2011**, *47*, 11686 – 11688.
[27] K. Tashiro, K. Konishi, T. Aida, *J. Am. Chem. Soc.* **2000**, *122*, 7921 – 7926.
[28] A. Sugasaki, M. Ikeda, M. Takeuchi, A. Robertson, S. Shinkai, *J. Chem. Soc. Perkin 1* **1999**, 3259 – 3264.
[29] S. Ogi, T. Ikeda, R. Wakabayashi, S. Shinkai, M. Takeuchi, *Chem. Eur. J.* **2010**, *16*, 8285 – 8290.
[30] M. Shibata, S. Tanaka, T. Ikeda, S. Shinkai, K. Kaneko, S. Ogi, M. Takeuchi, *Angew. Chem. Int. Ed.* **2013**, *52*, 397 – 400; *Angew. Chem.* **2013**, *125*, 415 – 418.
[31] K.-i. Yamashita, T. Yamanaka, N. Sakata, T. Ogawa, *Chem. Asian J.* **2018**, *13*, 1692 – 1698.
[32] M. Damjanović, T. Morita, K. Katoh, M. Yamashita, M. Enders, *Chem. Eur. J.* **2015**, *21*, 14421 – 14432.
[33] J. Otsuki, Y. Komatsu, D. Kobayashi, M. Asakawa, K. Miyake, *J. Am. Chem. Soc.* **2010**, *132*, 6870 – 6871.
[34] T. Ikeda, T. Tsukahara, R. Iino, M. Takeuchi, H. Noji, *Angew. Chem. Int. Ed.* **2014**, *53*, 10082 – 10085; *Angew. Chem.* **2014**, *126*, 10246 – 10249.
[35] T. Komeda, H. Isshiki, J. Liu, Y.-F. Zhang, N. Lorente, K. Katoh, B. K. Breedlove, M. Yamashita, *Nat. Commun.* **2011**, *2*, 217.
[36] N. Ishikawa, M. Sugita, T. Ishikawa, S. Y. Koshihara, Y. Kaizu, *J. Am. Chem. Soc.* **2003**, *125*, 8694 – 8695.
[37] M. Urdampilleta, S. Klyatskaya, J. P. Cleuziou, M. Ruben, W. Wernsdorfer, *Nat. Mater.* **2011**, *10*, 502 – 506.
[38] M. Ganzhorn, S. Klyatskaya, M. Ruben, W. Wernsdorfer, *Nat. Nanotechnol.* **2013**, *8*, 165 – 169.
[39] S. Takamatsu, N. Ishikawa, *Polyhedron* **2007**, *26*, 1859 – 1862.
[40] S. Takamatsu, T. Ishikawa, S.-Y. Koshihara, N. Ishikawa, *Inorg. Chem.* **2007**, *46*, 7250 – 7252.
[41] N. Ishikawa, Y. Mizuno, S. Takamatsu, T. Ishikawa, S.-Y. Koshihara, *Inorg. Chem.* **2008**, *47*, 10217 – 10219.

[42] T. Fukuda, K. Hata, N. Ishikawa, *J. Am. Chem. Soc.* **2012**, *134*, 14698 – 14701.
[43] K. Katoh, Y. Horii, N. Yasuda, W. Wernsdorfer, K. Toriumi, B. K. Breedlove, M. Yamashita, *Dalton Trans.* **2012**, *41*, 13582 – 13600.
[44] Y. Horii, K. Katoh, N. Yasuda, B. K. Breedlove, M. Yamashita, *Inorg. Chem.* **2015**, *54*, 3297 – 3305.
[45] Y. Horii, K. Katoh, K. Sugimoto, R. Nakanishi, B. K. Breedlove, M. Yamashita, *Chem. Eur. J.* **2019**, *25*, 3098 – 3104.
[46] Y. Horii, K. Katoh, G. Cosquer, B. K. Breedlove, M. Yamashita, *Inorg. Chem.* **2016**, *55*, 11782 – 11790.
[47] K. Katoh, T. Kajiwara, M. Nakano, Y. Nakazawa, W. Wernsdorfer, N. Ishikawa, B. K. Breedlove, M. Yamashita, *Chem. Eur. J.* **2011**, *17*, 117 – 122.
[48] G. Sheldrick, *Acta Crystallogr. Sect. A* **2008**, *64*, 112 – 122.
[49] I. Bertini, C. Luchinat, *Coord. Chem. Rev.* **1996**, *150*, 29 – 75.
[50] M. Enders, in *Modeling of Molecular Properties* (Ed.: P. Comba), Wiley-VCH Verlag GmbH & Co. KGaA, Weinheim, Germany, **2011**.
[51] G. N. La Mar, *NMR of Paramagnetic Molecules—Principles and Applications*, Academic Press, INC., New York and London, **1973**.
[52] B. Bleaney, *J. Magn. Reson.* **1972**, *8*, 91 – 100.
[53] M. Damjanovic, K. Katoh, M. Yamashita, M. Enders, *J. Am. Chem. Soc.* **2013**, *135*, 14349 – 14358.
[54] T. Morita, M. Damjanović, K. Katoh, Y. Kitagawa, N. Yasuda, Y. Lan, W. Wernsdorfer, B. K. Breedlove, M. Enders, M. Yamashita, *J. Am. Chem. Soc.* **2018**, *140*, 2995 – 3007.
[55] H. J. Hogben, M. Krzystyniak, G. T. Charnock, P. J. Hore, I. Kuprov, *J. Magn. Reson.* **2011**, *208*, 179 – 194.
[56] A. D. Becke, *J. Chem. Phys.* **1993**, *98*, 5648 – 5652.
[57] C. Lee, W. Yang, R. G. Parr, *Phys. Rev. B* **1988**, *37*, 785 – 789.
[58] R. Ditchfield, W. J. Hehre, J. A. Pople, *J. Chem. Phys.* **1971**, *54*, 724 – 728.
[59] M. Dolg, H. Stoll, H. Preuss, R. M. Pitzer, *J. Phys. Chem. C* **1993**, *97*, 5852 – 5859.
[60] N. Ishikawa, Y. Kaizu, *Chem. Phys. Lett.* **1993**, *203*, 472 – 476.
[61] N. Ishikawa, Y. Kaizu, *J. Phys. Chem. A* **2000**, *104*, 10009 – 10016.
[62] K. Wang, D. Qi, H. Wang, W. Cao, W. Li, T. Liu, C. Duan, J. Jiang, *Chem. Eur. J.* **2013**, *19*, 11162 – 11166.
[63] S. Lee, K.-i. Yamashita, N. Sakata, Y. Hirao, K. Ogawa, T. Ogawa, *Chem. Eur. J.* **2019**, *25*, 3240 – 3243.
[64] L. Ungur, L. F. Chibotaru, *Phys. Chem. Chem. Phys.* **2011**, *13*, 20086 – 20090.
[65] J. J. Baldoví, J. J. Borrás-Almenar, J. M. Clemente-Juan, E. Coronado, A. Gaita-Ariño, *Dalton Trans.* **2012**, *41*, 13705 – 13710.

Manuscript received: March 19, 2020
Revised manuscript received: May 7, 2020
Accepted manuscript online: May 19, 2020
Version of record online: June 18, 2020

